2024 European Control Conference (ECC)
June 25-28, 2024. Stockholm, Sweden

# Iterative interaction decoupling for multivariate time-varying systems applied to a Gravitational Wave Detector

Mathyn van Dael[1,2], Gert Witvoet[1,3], Bas Swinkels[3], Diego Bersanetti[4], Manuel Pinto[5], Julia Casanueva[5], Maddalena Mantovani[5], Piernicola Spinicelli[5], Camilla de Rossi[5] and Tom Oomen[1,6]

***Abstract*— Some of the feedback loops in the Advanced Virgo+ Gravitational Wave detector exhibit strong coupling and this coupling also varies over time. This paper presents a method to decouple the loops using a decoupling matrix, removing restrictions on the attainable performance of the feedback loops. The presented method performs batch-wise identification of the coupling matrix using only a single sinusoid per loop as perturbation by exploiting the specific structure of the plant to interpolate between frequency bins. The presented method is implemented on AdV+ and is shown to lead to significant decoupling of the loops and to keep the interaction terms low over time.**

## I. INTRODUCTION

Gravitational Wave (GW) detectors such as Advanced Virgo+ (AdV+) [1] and Advanced LIGO+ (aLIGO+) [2] are large complex optomechatronic systems capable of measuring spatial fluctuations in the order of $1 \times 10^{-18}\,\mathrm{m}$ over a length of several kilometers. These detectors employ interferometry to measure these spatial fluctuations, requiring the relative distance between all the optical components to be actively controlled through feedback loops with up to picometer precisions [3]. The error signals for these feedback loops are derived from frequency-modulated monochromatic light propagating through the detector and demodulated at one of the photodiodes [4], [5]. These error signals inherently measure a combination of degrees of freedom (DoFs), with the best error signal for a DoF thus predominantly measuring only that DoF. In most cases error signals are found for which the coupling to other DoFs can be neglected, allowing for SISO control design methods. In previous work [6], it has however been shown that presently the coupling in AdV+ for three DoFs is of such significance that MIMO design tools are required to guarantee stability and that these interaction terms furthermore vary over time. The combination of the large interaction terms and their time-varying behavior poses limitations on the attainable control performance and therefore indirectly also the detector sensitivity.

Although some research has been done on addressing the problem of strongly coupled and time-varying feedback loops in GW detectors, to the knowledge of the authors no solution exists that addresses this problem in a time-efficient manner without posing limitations on the detector sensitivity. The most common approach so far has been to simply extend the search of optimal modulation frequencies and photodiodes to find a better-decoupled error signal, but this solution is very cumbersome in terms of simulation time with no guarantees that a better error signal can be found and whether that is practically feasible. In terms of a control-related solution, previous work [6] presented a method to derive SISO design requirements to obtain MIMO stability and robustness. The downside of this method is however that it poses limits on the attainable detector sensitivity due to the required stability margins for the SISO loops. Beyond these two methods, no solution has been presented in the literature that successfully addresses this problem.

In answer to this, this paper presents a decoupling procedure that iteratively updates the decoupling matrix to compensate for the time-varying couplings induced by the sensors. The contribution of this paper is two-fold. The first is the derivation of an identification scheme that allows the identification of the coupling matrix using only a pure sinusoid injected in each DoF, each of which is at a distinct frequency. This identification scheme is then used to determine the decoupling matrix which will show to significantly reduce the interaction terms. The second contribution is the practical implementation of the proposed method on the complete AdV+ detector, adjusting the algorithm to accommodate certain implementation requirements. Experimental verification of the proposed method is presented through the comparison of the measured interaction terms on the complete AdV+ with and without the proposed algorithm, which will illustrate the practical effectiveness of the proposed method.

The outline of this paper is as follows. In Section II, a description of the AdV+ detector is given and the problem addressed in this paper is formally formulated. Section III then derives the identification procedure used after which implementation aspects and the experimental results from AdV+ are presented in Section IV. A conclusion on the presented work is given in Section V.

## II. PROBLEM FORMULATION

### A. System description

Large-scale interferometers measure GWs by monitoring the interference pattern of two orthogonal beams of light, which expand and contract as a result of a passing GW. A top view as well as the optical configuration of AdV+ is

[1]Eindhoven University of Technology, dept. of Mechanical Engineering, Control Systems Technology, Eindhoven, The Netherlands m.r.v.dael@tue.nl
[2]Nikhef, Amsterdam, The Netherlands
[3]TNO, Optomechatronics Department, Delft, The Netherlands
[4]INFN, Sezione di Genova, I-16146 Genova, Italy
[5]European Gravitational Observatory (EGO), I-56021 Cascina, Pisa, Italy
[6]Delft Center for Systems and Control, Delft University of Technology, Delft, The Netherlands

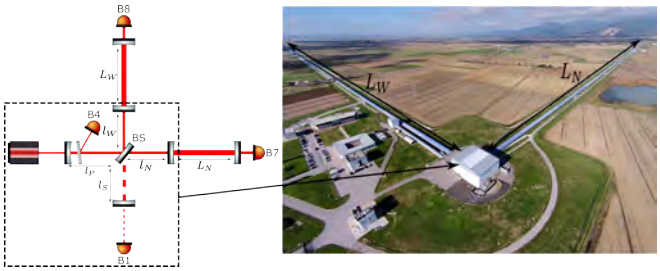


Fig. 1. Part of the optical configuration of AdV+ for the next science run (left) and picture of AdV+ (right). The B1 photodiode measures the interference pattern between the two arms ($l_W + L_W$ and $l_N + L_N$), which change in length with opposite signs when a GW passes. The two tunnels with length $L_W$ and $L_N$ are 3 km long in AdV+.

depicted in Fig. 1. The white building contains the laser, the Beam Splitter (BS) that creates the orthogonal beams and the B1 photodiode that measures the interference pattern, among other optics. The two 3 km long orthogonal arms $L_W$, $L_N$ predominantly determine the interference and change with opposing length when a GW passes.

The length changes of the two arms $L_W$, $L_N$ are in the order of $1 \times 10^{-18}$ m. The extreme precision of the relative length distances between mirrors and their angular orientations are thus required to distinguish length changes due to a passing GW from other environmental effects. All these DoFs are controlled using feedback loops that extract an error signal based on the powers on the photodiodes [5] and act on the longitudinal or angular positions of the mirrors. The DoFs furthermore exhibit a certain level of interaction, which is typically minimized by appropriately choosing the error signals sensitive to predominantly a single DoF [4]. While often possible, some of the loops still exhibit significant interaction, requiring more advanced tools beyond standard SISO control design to guarantee stability and performance. Three of the most important DoFs subject to this problem are analyzed next.

### B. Time-varying coupling

This paper focuses on three of the longitudinal DoFs in AdV+, commonly referred to as the Central Interferometer (CITF) DoFs and given by

$$\begin{aligned} L_{\text{MICH}} &= l_N - l_W, \\ L_{\text{PRCL}} &= l_P + \frac{l_N + l_W}{2}, \\ L_{\text{SRCL}} &= l_S + \frac{l_N + l_W}{2}, \end{aligned} \tag{1}$$

where MICH is an abbreviation for Michelson and refers to the difference in length between $l_N$ and $l_W$, PRCL for Power Recycling Cavity length since it reflects the power reflected by the BS back into the interferometer, and SRCL for Signal Recycling Cavity length for the same reasoning.

These DoFs are actively controlled using Voice Coils on the back of the mirrors to accurately change their position, and the error signals for the feedback loops are obtained through frequency-modulated light measured on the different

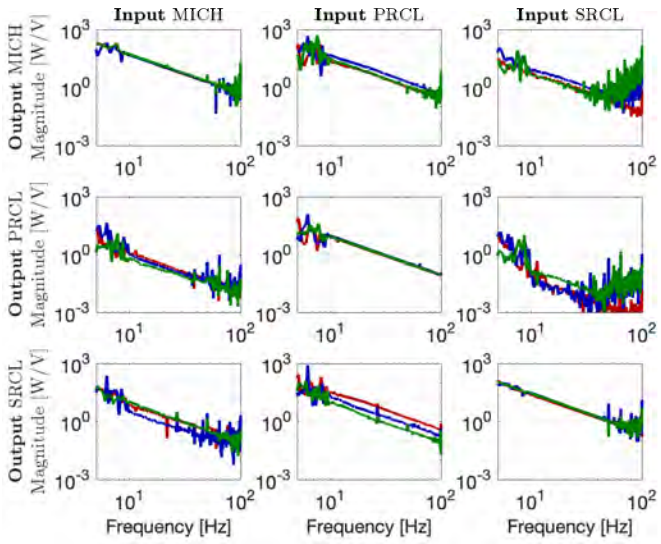


Fig. 2. Bode magnitude plot of three different Frequency Response Function measurements (—), (—) and (—) of $H$, measured at least two weeks apart.

photodiodes. The system dynamics of the CITF DoFs are formulated as

$$H(j\omega) = G_i A(j\omega), \tag{2}$$

where $A \in \mathcal{C}^{n\times n}$ is the stable rational transfer matrix translating actuator voltages to a change in length of the DoFs, which also contains a static coordinate transformation from mirror positions to the DoFs as formulated in (1), and $G_i \in \mathbb{R}^{n\times n}$ the optical plant relating the mirror motions to the powers measured on the photodiodes. In practice, the optical plant $G$ also contains a single pole per DoF of which the frequency depends on the optics for each DoF. However, for the DoFs discussed in this paper, these poles are far above the frequency range of interest, which is why the optical plant is approximated by a real matrix. The subscript furthermore denotes a realization of the time-varying matrix $G$, i.e.

$$G(t) = G_i \,\forall\, t \in [t_1\, t_2], \tag{3}$$

where $G(t)$ is the matrix $G$ varying over time. Throughout this paper $A$ is considered to be diagonal over the frequency range of interest, assuming that the actuation is perfectly decoupled. The optical plant $G$ is known to be strongly coupled since the photodiodes measure a combination of the different frequency-modulated light beams [4], [5].

In Fig. 2, the Frequency Response Matrix (FRM) of the three DoFs is shown, measured at three different time instances. Not only are the off-diagonal terms large in magnitude, but they also fluctuate over time, where the time dependency stems from thermal transients and changes in the relative alignment between the mirrors which changes the optical response over time.

In [6], it has been shown that the level of interaction is of such significance that MIMO control design tools are

necessary to guarantee stability and robustness. The method proposed in [6] to deal with the time-varying interaction terms exploits the plant structure to derive requirements on the SISO stability margins. While effective, the imposed requirements on the stability margins proved to pose limitations on the attainable RMS and roll-off of the loops thus also limiting the detector sensitivity. A solution that does not pose these limitations is therefore desired.

### C. Reducing interaction through decoupling

The method pursued in this paper is to use static decoupling [7] and iteratively update the coefficients of the decoupling matrix to cope with the time-varying plant aspects. This frees the SISO loops from any restrictions on the stability margins due to the interaction terms and is furthermore very easy to implement from a practical standpoint. Since the actuation $A(j\omega)$ is assumed to be diagonal, perfect decoupling is achieved when

$$T_y = G_i^{-1}. \tag{4}$$

However, to implement this decoupling strategy, continuous identification of $G$ is required since the coupling matrix $G$ is time-varying. Continuous noise injections such as the experiments done to obtain 2 are not feasible since they spoil the detector sensitivity. In AdV+, a single so-called line is injected in each DoF for monitoring purposes, which is a single sinusoid at a distinct frequency. These single sinusoids in each DoF will be used to continuously estimate $G$ and implement the static decoupling matrix $T_y$.

### D. Problem formulation

The problem addressed in this paper is to decouple the CITF DoFs using batch-wise identification of the optical coupling matrix $G$ and implementing its inverse in an output matrix $T_y$ since the coupling stems from the sensing mechanism. The identification scheme has to work given the following requirements

- **R1:** Only a single line per DoF is available as an external perturbation, which is at arbitrary but non-identical frequencies.
- **R2:** An estimation method is required that does not require knowledge of the controller
- **R3:** Updates of the output matrix $T_y$ may not introduce significant transients in the loops.

While the controllers of each loop are known, the requirement **R2** is set for practical purposes since the controllers are regularly changed and it is not straightforward to automatically read the current controllers in the software. The assumption is furthermore made that the structure of the frequency response of $A(j\omega)$ is known over the frequency range of interest. The objective of this work is thus to derive a decoupling scheme that satisfies these requirements.

## III. IDENTIFICATION USING INTERPOLATION

This section derives the identification procedure that estimates the optical plant using a single line per DoF.

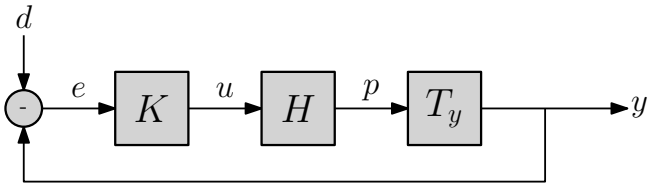


Fig. 3. Block diagram of the control system used to control the LSC degrees of freedom in AdV+.

### A. Identification setting

A block diagram of the control setting considered here is shown in Fig. 3. A plant $H(j\omega)$ of dimension $n \times n$ is considered which satisfies the following structure

$$H(j\omega) = h(j\omega) \cdot \mathcal{H}, \tag{5}$$

with $h(j\omega)$ a SISO transfer function and $\mathcal{H} \in \mathbb{R}^{n\times n}$ a real matrix. The motivation for this specific structure in the context of AdV+ will be given in Section IV-A. The input to the plant is the control signal $u \in \mathbb{R}^n$, generated by a controller $K \in \mathcal{R}^{n\times n}$ from the error signal $e \in \mathbb{R}^n$. The perturbation $d \in \mathbb{R}^n$ are the lines for each DoF, i.e.

$$d = \begin{bmatrix} A_1 \cos(\omega_1 t) \\ A_2 \cos(\omega_2 t) \\ \vdots \\ A_n \cos(\omega_n t) \end{bmatrix}, \tag{6}$$

where $\omega_i$, $i = 1, 2, \ldots, n$ are the excitation frequencies which are all distinct and $A_i$ the respective amplitudes of the line. The system output $y \in \mathbb{R}^n$ is a change of coordinates with respect to the sensor outputs $p \in \mathbb{R}^n$, transformed by the real matrix $T_y \in \mathbb{R}^{n\times n}$. Throughout the first part, $T_y = I$ is assumed and therefore $y = p$. As mentioned, $h(j\omega)$ is furthermore assumed to be available, which could be obtained from measurements or modeling. The objective is then to identify $\mathcal{H}$ using only the perturbation $d$.

The discrete time signals $\hat{x}(lT_s)$ with $N$ the length of the data trace are used for the identification, which is subject to noise from other perturbations (e.g. sensor or input noise) and thus estimates of the signal $x$. The DFT of these discrete time signals is defined as [8]

$$X(k) = \frac{1}{\sqrt{N}} \sum_{l=0}^{N-1} x(lT_s) e^{-j2\pi lk/N}. \tag{7}$$

### B. Identification using interpolation

Suppose that multiple experiments can be performed for an $n \times n$ system, then a common approach is to perform $n$ experiments in which orthogonal multisines are consecutively injected. The $\boldsymbol{U}$ and $\boldsymbol{Y}$ matrices are then constructed according to [8]

$$\boldsymbol{X(k)} = \begin{bmatrix} X_1^1(k) & X_1^2(k) & \ldots & X_1^n(k) \\ X_2^1(k) & X_2^2(k) & \ldots & X_2^n(k) \\ \vdots & \vdots & \ddots & \vdots \\ X_n^1(k) & X_n^2(k) & \ldots & X_n^n(k) \end{bmatrix} \tag{8}$$

for $\boldsymbol{X} = \boldsymbol{U}, \boldsymbol{Y}$ and where $X_n^m(k)$ denotes output $n$ in experiment $m$ at the excited frequency bin $k$. The plant $H$ is then obtained by computing

$$H(k) = \boldsymbol{Y}(k)\boldsymbol{U}(k)^{-1} \tag{9}$$

for every frequency bin $k$. If the same procedure is applied by considering each excitation signal as a separate experiment then the following matrix is constructed

$$\boldsymbol{X} = \begin{bmatrix} X_1^{k_1} & X_1^{k_2} & \dots & X_1^{k_n} \\ X_2^{k_1} & X_2^{k_2} & \dots & X_2^{k_n} \\ \vdots & \vdots & \ddots & \vdots \\ X_n^{k_1} & X_n^{k_2} & \dots & X_n^{k_n} \end{bmatrix} = \begin{bmatrix} X^{k_1} & X^{k_2} & \dots X^{k_n}, \end{bmatrix}, \tag{10}$$

with $X^{k_m}$ the DFT of the time domain vector $x$ evaluated at the discrete frequency bin $k_m$ of $\omega_m$. Solving for $H$ using (9) however is not possible since the columns are evaluated at different frequency bins $k_i$. This problem is solved by exploiting the known structure of $h(j\omega_{k_m})$. Consider the following direct input-output relation

$$\begin{bmatrix} Y_1^{k_m} \\ Y_2^{k_m} \\ \vdots \\ Y_n^{k_m} \end{bmatrix} = h(j\omega_{k_m}) \cdot \mathcal{H} \cdot \begin{bmatrix} U_1^{k_m} \\ U_2^{k_m} \\ \vdots \\ U_n^{k_m} \end{bmatrix} \tag{11}$$

for each DoF and its respective excitation $m = 1, 2, \dots, n$. Multiplying both sides by $1/h(j\omega_{k_m})$ yields

$$Y^{k_m}/h(j\omega_{k_m}) = \mathcal{H}U^{k_m}, \tag{12}$$

where $\mathcal{H}$ is now the only unknown since $U^{k_m}$, $Y^{k_m}$ are computed based on data and $h(j\omega_{k_m})$ is assumed known. The term on the left can thus be computed for each excited line permutation, subsequently allowing the construction of the full matrix for all $n$ excitation signals

$$\underbrace{\begin{bmatrix} Y_1^{k_1} & Y_1^{k_2} & \dots & Y_1^{k_n} \\ Y_2^{k_1} & Y_2^{k_2} & \dots & Y_2^{k_n} \\ \vdots & \vdots & \ddots & \vdots \\ Y_n^{k_1} & Y_n^{k_2} & \dots & Y_n^{k_n} \end{bmatrix}}_{=\boldsymbol{Y}} \cdot \boldsymbol{N} = \mathcal{H} \cdot \underbrace{\begin{bmatrix} U_1^{k_1} & U_1^{k_2} & \dots & U_1^{k_n} \\ U_2^{k_1} & U_2^{k_2} & \dots & U_2^{k_n} \\ \vdots & \vdots & \ddots & \vdots \\ U_n^{k_1} & U_n^{k_2} & \dots & U_n^{k_n} \end{bmatrix}}_{=\boldsymbol{U}}, \tag{13}$$

with

$$\boldsymbol{N} = \begin{bmatrix} \frac{1}{h(j\omega_{k_1})} & 0 & \dots & 0 \\ 0 & \frac{1}{h(j\omega_{k_2})} & \dots & 0 \\ \vdots & \vdots & \ddots & \vdots \\ 0 & 0 & \dots & \frac{1}{h(j\omega_{k_n})}. \end{bmatrix} \tag{14}$$

An equation containing two matrices of signals analogous to (8) is now obtained, allowing to solve for $\mathcal{H}$ by computing

$$\mathcal{H} = \boldsymbol{Y}\boldsymbol{N} \cdot \boldsymbol{U}^{-1}. \tag{15}$$

The method essentially normalizes the output DFTs with respect to their different frequencies through $\boldsymbol{N}$ and by using the same method as initially described for multisines to obtain an estimate of $\mathcal{H}$. Since lines are used, closed-loop aspects relating to input-output correlation do not form a problem, allowing open-loop identification which greatly simplifies the identification scheme. The method furthermore also does not require knowledge of the controller, thus satisfying **R3**. Finally, it correctly incorporates MIMO aspects to obtain an unbiased estimate of $\mathcal{H}$, with respect to doing e.g. element-wise division of $\boldsymbol{Y}$, $\boldsymbol{U}$ which would lead to biased estimates [9]. This method will be used to continuously identify the optical plant $G$ in AdV+ and update its decoupling matrix $T_y$.

## IV. Experimental results

The proposed decoupling method is implemented on the AdV+ detector and this section presents the implementation and experimental results based on data from the AdV+ detector.

### A. Implementation of decoupling on AdV+

The objective is to decouple the three CITF DoFs between 1 and 100 Hz since the bandwidths of the loops are in this frequency range. Since $G$ is time-varying, the proposed identification method is used to continuously identify realizations of $G$, i.e. $G_i$, and update $T_y$ accordingly. Here it is thus assumed that the fluctuations of $G$ are sufficiently slow such that (3) holds. While it is known that this is in practice not true, the assumption is made that the identification time is sufficiently short such that the fluctuations in the period of the identification can be neglected. This assumption solely stems from practical experiences, since the complexity of the system and the number of variables contributing to the transients are so large that it is too difficult to model these effects or provide sensible bounds on e.g. the magnitude or the time constants of the fluctuations.

The actuation dynamics $A(j\omega)$ of the CITF DoFs are modeled as a harmonic oscillator with a resonance frequency below 1 Hz, representing the dynamics from applying a force to a softly suspended mirror to its response. Above this frequency, the dynamics have a $-2$ slope and combined with the real matrix $G$, the plant dynamics can thus be approximated by a $-2$ slope, i.e.,

$$H(j\omega) = G_i \frac{1}{(j\omega)^2}, \tag{16}$$

which corresponds to the dynamic behavior observed in Fig. 2 and satisfies the assumed structure in (5). Each DoF has a single line injected slightly above the bandwidth of the loop, which during the performed experiments were at respectively 21.7, 64.4 and 26.6 Hz for the MICH, PRCL and SRCL loops. The fundamental frequency (i.e. the largest common divisor of the line frequencies which ensures that the signal in the DFT is in a single frequency bin) of the lines is at 0.1 Hz, so a measurement time of 180 s is taken to average over 18 periods. The identification method as defined in III is used

to estimate $\hat{G}^{\star^{-1}}$. The signals $\hat{u}(lT_s), \hat{y}(lT_s)$ are measured and an estimate of the decoupled plant is obtained through

$$\underbrace{\begin{bmatrix} Y_{\mathrm{M}}^{k_{\mathrm{M}}} & Y_{\mathrm{M}}^{k_{\mathrm{P}}} & Y_{\mathrm{M}}^{k_{\mathrm{S}}} \\ Y_{\mathrm{P}}^{k_{\mathrm{M}}} & Y_{\mathrm{P}}^{k_{\mathrm{P}}} & Y_{\mathrm{P}}^{k_{\mathrm{S}}} \\ Y_{\mathrm{S}}^{k_{\mathrm{M}}} & Y_{\mathrm{S}}^{k_{\mathrm{P}}} & Y_{\mathrm{P}}^{k_{\mathrm{S}}} \end{bmatrix}}_{=\boldsymbol{Y}} \cdot \boldsymbol{N} = T_y^{\mathrm{curr}} \cdot \tilde{G}^{\star} \cdot \underbrace{\begin{bmatrix} U_{\mathrm{M}}^{k_{\mathrm{M}}} & U_{\mathrm{M}}^{k_{\mathrm{P}}} & U_{\mathrm{M}}^{k_{\mathrm{S}}} \\ U_{\mathrm{P}}^{k_{\mathrm{M}}} & U_{\mathrm{P}}^{k_{\mathrm{P}}} & U_{\mathrm{P}}^{k_{\mathrm{S}}} \\ U_{\mathrm{S}}^{k_{\mathrm{M}}} & U_{\mathrm{S}}^{k_{\mathrm{P}}} & U_{\mathrm{S}}^{k_{\mathrm{S}}} \end{bmatrix}}_{=\boldsymbol{U}}, \tag{17}$$

where e.g. $Y_{\mathrm{M}}^{k_{\mathrm{M}}}$ is DFT of the MICH output computed at the frequency bin of the MICH line $k_{\mathrm{M}}$ and

$$\boldsymbol{N} = \begin{bmatrix} (j\omega_{k_{\mathrm{M}}})^2 & 0 & 0 \\ 0 & (j\omega_{k_{\mathrm{P}}})^2 & 0 \\ 0 & 0 & (j\omega_{k_{\mathrm{S}}})^2 \end{bmatrix}. \tag{18}$$

The estimate of the new coupling matrix is then given by

$$\hat{G}_i^{\mathrm{new}} = T_y^{\mathrm{curr}} \cdot \hat{G}_i = \boldsymbol{Y}\boldsymbol{N} \cdot \boldsymbol{U}^{-1} \tag{19}$$

and the new $T_y$ matrix becomes the inverse of $\hat{G}_i^{\mathrm{new}}$.

A method is now available to estimate $T_y$ using a perturbation satisfying **R1** and an identification scheme satisfying **R2**. To meet **R3**, i.e. avoid large transients in the loops resulting from updates of $T_y$, the following update law is used

$$T_y(m) = T_y^{\mathrm{old}} + \frac{m}{F_s \cdot t_{\mathrm{ramp}}} \left(T_y^{\mathrm{new}} - T_y^{\mathrm{old}}\right), \tag{20}$$

with $F_s$ the sampling time and $t_{\mathrm{ramp}}$ the time used to switch from the old to the new decoupling matrix. The ramp preserves the relative scaling of the values in the matrix, ensuring that the coupling doesn't worsen throughout the switching of the decoupling matrix without inducing a large transient in the system due to a jump in values in $T_y$. This property is proven by considering a static coupling matrix $G_i \in \mathbb{R}^{n\times n}$. The coupling during the transient from the old to the new $T_y$ matrix is given by

$$G_i^{\mathrm{dec}}(m) = G_i \cdot T_y^{\mathrm{old}} + \alpha(m) G_i \left(T_y^{\mathrm{new}} - T_y^{\mathrm{old}}\right), \tag{21}$$

with

$$\alpha(m) = \frac{m}{F_s \cdot t_{\mathrm{ramp}}} \in [0,\ 1]. \tag{22}$$

Rewriting (21) to

$$G_i^{\mathrm{dec}}(m) = (1-\alpha(m)) G_i T_y^{\mathrm{old}} + \alpha(m) G_i T_y^{\mathrm{new}} \tag{23}$$

and on the condition that the following holds

$$(G_i T_y^{\mathrm{new}})^{b,c} < (G_i T_y^{\mathrm{old}})^{b,c} \ \forall\, b, c, \tag{24}$$

i.e., each element of the decoupled plant with the new decoupling matrix is smaller than the corresponding element with the old decoupling matrix, proves that

$$G_i^{\mathrm{dec}^{b,c}}(m) < G_i^{\mathrm{dec}^{b,c}}(m-1) \ \ \forall\, b, c, m, \tag{25}$$

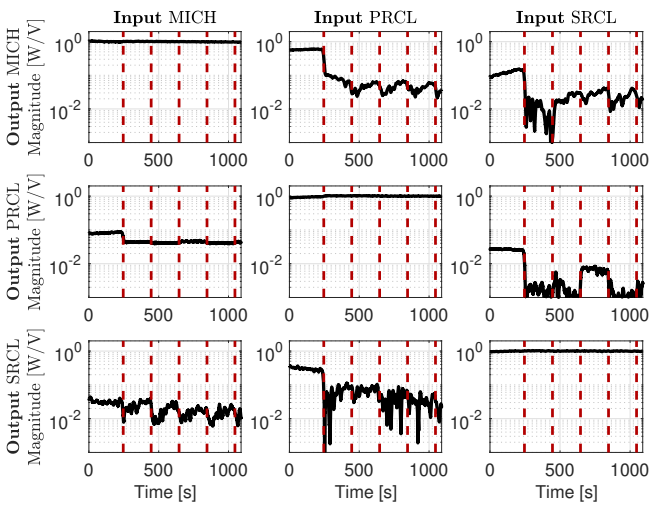


Fig. 4. Measured estimate of the coupling matrix $G(t)$ over time on AdV+. The time instances indicated by the vertical dashed lines show when the output matrix $T_y$ is updated. The off-diagonal entries of $G(t)$ are shown to decrease after each update and rise in amplitude in between updates.

where $b, c$ denotes the row and column respectively of the matrix. The aforementioned decoupling procedure is implemented on the AdV+ detector and experimental results are reported in the next two subsections.

### *B. Decoupling over time*

To evaluate the coupling over time, the same identification method is used to obtain a moving average estimate of $T_y G(t)$. Each time domain signal is therefore multiplied by the Euler coefficient at each line frequency, i.e.,

$$\tilde{x}^{k_m} = x(lT_s) \cdot e^{-j2\pi k/N}, \tag{26}$$

after which a moving average is applied

$$X_{\mathrm{ma}}^{k_m}(l) = \frac{1}{V+1} \sum_{v=0}^{V} \tilde{x}^{k_m}(v) q^{-v}, \tag{27}$$

with $q$ the shift operator, $V$ the number of coefficients and $x = \hat{u},\ \hat{y}$. The variable $X_{\mathrm{ma}}^{k_m}(l)$ is then a moving average on the DFT bin $k$ of signal $\hat{x}$. The same identification method is then applied over this moving average to estimate $T_y G(t)$.

A plot of this estimate is shown in Fig. 4. At time $t = 0$, no decoupling is applied. The $T_y$ matrix is then updated every $180\,\mathrm{s}$, highlighted by the vertical red dashed lines, according to the implementation procedure presented in Section IV-A. The off-diagonal elements are shown to be significantly decreased after the first iteration, where they are close to their minimum level. In between iterations, some of the terms, e.g., the $1,2$ and $1,3$ element, noticeably increase between iterations, highlighting the necessity of the iterative procedure to keep the couplings sufficiently small.

### *C. Decoupling quality*

To assess whether the coupling is indeed increased over the complete frequency range of interest, the frequency response

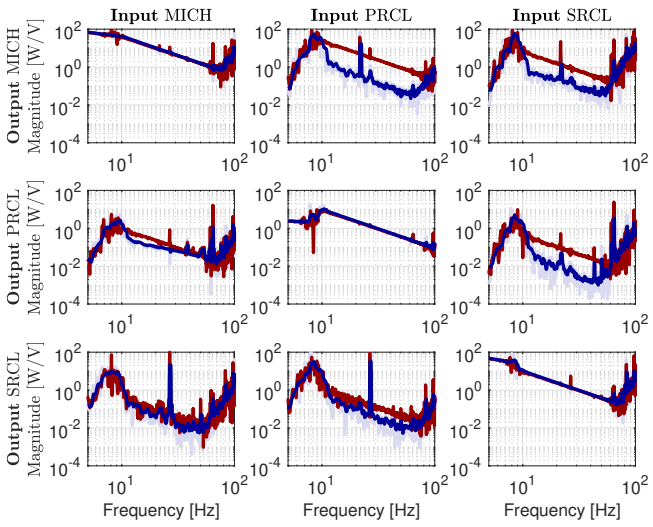


Fig. 5. Frequency Response Matrix of the plant $H$ of the CITF DoFs on AdV+. (—) No decoupling is applied, i.e. $T_y = I$, and (—) Decoupling is applied. Note that the transparent blue line is the original measured Frequency Response Matrix and the opaque version is a smoothed version to better illustrate the performance improvement. The couplings in all off-diagonal entries are decreased using the new method, with up to a factor of 20 in e.g. the PRCL to MICH element.

is measured without and with the decoupling procedure. The interferometer has first been left to converge to a more steady state in which most of the thermal transient has passed and the alignment of the mirrors has converged to their final positions. The MIMO frequency response is then measured using white noise band-passed between 10 and 50 Hz. Two iterations of the decoupling procedure were then performed after which another set of noise injections was done.

The measured MIMO frequency response for both cases is depicted in Fig. 5. The decoupling method is shown to decrease the coupling levels by up to a factor of 20 over the identified frequency response. The only outlier is the $2, 1$ element, where the applied decoupling seems to be somewhat less effective compared to the other elements towards 50 Hz. This seems to stem from some unknown and unmodelled dynamics, which do not satisfy the plant structure assumed in (16). The level of coupling is nevertheless still sufficiently low for this not to pose a problem.

## V. DISCUSSION

A combined identification scheme and iterative decoupling procedure have been presented in this paper, which performs batch-wise identification of the coupling using pre-existing perturbation signals in the AdV+ detector to derive a static decoupling matrix. Experimental verification of the proposed method on the complete AdV+ detector has shown a significant reduction of the interaction terms over the complete frequency range of interest, as well as the effectiveness of the iterative updating scheme in keeping the interaction terms below a threshold over time. While exact requirements on the required level of decoupling are out of scope for this work, the presented method has been shown to lead to sufficiently low coupling levels such that no restrictions are imposed on the SISO design loops anymore.

Future work may focus on identifying the limiting factors in further reducing the coupling, as this might be of interest when applying this technique to other DoFs. Additionally, a generic structure for the plant has been assumed, which might be too restricting for certain DoFs. Further research could focus on generalizing this technique to DoFs with different structures in terms of their coupling. Finally, the consequence of using static decoupling matrices on noise propagation to the output of the detector might be of interest for future work, since minimizing these noise propagations is an essential part of the system.

## ACKNOWLEDGMENT

The authors gratefully acknowledge the Italian Istituto Nazionale di Fisica Nucleare (INFN), the French Centre National de la Recherche Scientifique (CNRS) and the Netherlands Organization for Scientific Research, for the construction and operation of the Virgo detector and the creation and support of the EGO consortium. The authors also gratefully acknowledge research support from these agencies as well as by the Spanish Agencia Estatal de Investigación, the Consellera d'Innovació, Universitats, Ciència i Societat Digital de la Generalitat Valenciana and the CERCA Programme Generalitat de Catalunya, Spain, the National Science Centre of Poland and the Foundation for Polish Science (FNP), the European Commission, the Hungarian Scientific Research Fund (OTKA), the French Lyon Institute of Origins (LIO), the Belgian Fonds de la Recherche Scientifique (FRS-FNRS), Actions de Recherche Concertées (ARC) and Fonds Wetenschappelijk Onderzoek – Vlaanderen (FWO), Belgium.

## REFERENCES

[1] F. Acernese *et al.*, "Advanced Virgo: a second-generation interferometric gravitational wave detector," *Class. Quant. Grav.*, vol. 32, no. 2, p. 024001, 2015.

[2] J. Aasi *et al.*, "Advanced LIGO," *Classical and Quantum Gravity*, vol. 32, no. 7, p. 074001, mar 2015.

[3] M. Valentini, "The longitudinal control for the Advanced Virgo Plus gravitational wave detector," Ph.D. dissertation, Trento U., 2023.

[4] D. Bersanetti, M. Boldrini, J. C. Diaz, A. Freise, R. Maggiore, M. Mantovani, and M. Valentini, "Simulations for the Locking and Alignment Strategy of the DRMI Configuration of the Advanced Virgo Plus Detector," *Galaxies*, vol. 10, no. 6, 2022.

[5] E. D. Black, "An introduction to pound-drever-hall laser frequency stabilization," *American Journal of Physics*, vol. 69, pp. 79–87, 2001.

[6] M. van Dael, G. Witvoet, B. Swinkels, M. Pinto, J. Casanueva, D. Bersanetti, M. Mantovani, M. Vardaro, and T. Oomen, "Design for interaction: Factorized nyquist based control design applied to a gravitational wave detector," *IFAC-PapersOnLine*, vol. 55, no. 37, pp. 107–112, 2022, 2nd Modeling, Estimation and Control Conference MECC 2022.

[7] J. Lee, D. Hyun Kim, and T. F. Edgar, "Static decouplers for control of multivariable processes," *AIChE Journal*, vol. 51, no. 10, pp. 2712–2720, 2005.

[8] R. Pintelon and J. Schoukens, *System Identification: A Frequency Domain Approach*. Wiley, 2012.

[9] E. Evers, R. Voorhoeve, and T. Oomen, "On frequency response function identification for advanced motion control," in *2020 IEEE 16th International Workshop on Advanced Motion Control (AMC)*, 2020, pp. 1–6.